

Tissue fusion over nonadhering surfaces

Vincent Nier^{a,1}, Maxime Deforet^{a,b,1}, Guillaume Duclos^{a,b,1}, Hannah G. Yevick^{a,b}, Olivier Cochet-Escartin^{a,b}, Philippe Marcq^{a,2}, and Pascal Silberzan^{a,b,2}

^aLaboratoire Physico-Chimie Curie, Institut Curie, Centre de Recherche, Paris Sciences et Lettres Research University, Centre National de la Recherche Scientifique, Université Pierre et Marie Curie, Sorbonne Universités, 75248 Paris, France and ^bLaboratoire PhysicoChimie Curie, Institut Curie, Equipe labellisée Ligue Contre le Cancer, 75248 Paris, France

Edited by Robert H. Austin, Princeton University, Princeton, NJ, and approved June 19, 2015 (received for review January 20, 2015)

Tissue fusion eliminates physical voids in a tissue to form a continuous structure and is central to many processes in development and repair. Fusion events in vivo, particularly in embryonic development, often involve the purse-string contraction of a pluricellular actomyosin cable at the free edge. However, in vitro, adhesion of the cells to their substrate favors a closure mechanism mediated by lamellipodial protrusions, which has prevented a systematic study of the purse-string mechanism. Here, we show that monolayers can cover well-controlled mesoscopic nonadherent areas much larger than a cell size by purse-string closure and that active epithelial fluctuations are required for this process. We have formulated a simple stochastic model that includes purse-string contractility, tissue fluctuations, and effective friction to qualitatively and quantitatively account for the dynamics of closure. Our data suggest that, in vivo, tissue fusion adapts to the local environment by coordinating lamellipodial protrusions and purse-string contractions.

wound closure | tissue fusion | purse string contraction | epithelial fluctuations

Tissue fusion is a frequent and important event during which two facing identical tissues meet and bridge collectively over a gap before merging into a continuous structure (1). Imperfect tissue fusion in embryonic development results in congenital defects for instance, in the palate, the neural tube, or the heart (1). Epithelial wound healing is another illustration of tissue fusion through which a gap in an epithelium closes to restore the integrity of the monolayer (2).

Model in vitro experiments have been developed using cell monolayers to study the different stages of healing from collective cell migration to the final stages of closure. In this context, we (3) and others (4, 5) have recently demonstrated that, for cells adhering to their substrate, and despite the presence of a contractile peripheral actomyosin cable at the free edge, the final stages of closure of wounds larger than a typical cell size result mostly from protrusive lamellipodial activity at the border. In that case, the function of the actin cable appears to be primarily to prevent the onset of migration fingers led by leader cells (6) at the free edge. Cell crawling has also been shown to have a major role in tissue fusion in vivo, for example during the closure of epithelial wounds in the *Drosophila* embryo (7).

However, in physiological developmental situations, there is often no underlying substrate to which lamellipodia can adhere to exert traction forces. This is the case, for instance, in neural tube formation (8) or in wound healing in the *Xenopus* oocyte (9). The generally well-accepted mechanism in these adhesion-free situations is the so-called purse-string mechanism in which the actomyosin cable at the edge of the aperture closes it by contractile activity (10). Note that the purse-string and the crawling mechanisms are not mutually exclusive (11) and may be involved at different stages of the closure (5, 12). In addition, “suspended” cohorts of cells, which do not interact with a substrate besides being anchored to a few discrete attachment points, are also observed in situations such as collective migration in cancer invasion (13).

Several experimental studies have documented protrusion-driven collective migration in vitro, but the purse-string mechanism has not been thoroughly investigated in model situations. Such an analysis imposes to suppress the contribution of the

protrusions to closure and, therefore, to conduct the experiments on nonadherent substrates.

In a seminal paper, fibroblast sheets were shown to grow and migrate with their sides anchored to thin glass fibers (14). More recent studies extended this observation to keratinocyte monolayers or epidermal stem cells bridging between microcontact-printed adhesive tracks (15, 16). However, despite recent advances emphasizing the role of tissue remodeling (17), the mechanism of closure of a suspended epithelium in the absence of these anchoring sites remains an open question. To address this point, we have studied the dynamics of gap closure in an unsupported epithelium in which the actomyosin cable and the suspended tissue could not adhere to the substrate. Purse-string contractility in the absence of protrusions was therefore studied on well-defined mesoscopic nonadherent patches within an adherent substrate.

Results

We studied the bridging of a monolayer over a well-defined non-adherent gap on adherent glass substrates patterned with strictly nonadhesive circular regions of radius R between 5 and 75 μm (Fig. 1A). The surface treatment kept its nonadherent properties for up to 3 wk in biological buffers (18, 19). To ensure we obtained reliable statistics, we worked with arrays of tens of nonadherent identical domains on which we cultured epithelial Madin Darby canine kidney (MDCK) cells (Fig. 1B) (20). Notably, MDCK cell sheets have been previously shown to remain functional when suspended over large distances in culture medium (21). Fusion processes in neighboring domains remained independent by imposing a space between each of at least 300 μm , a distance larger than the velocity correlation length measured independently for

Significance

Tissue fusion is a frequent and important event in embryonic development during which two facing identical tissues meet and bridge collectively over a gap before merging into a continuous structure. Illustrations of tissue fusion include the formation of the palate or epithelial wound healing. In vivo fusion events, particularly in embryonic development, often involve the purse-string contraction of a pluricellular actomyosin cable present at the free edge. By studying the fusion of a monolayer over imprinted nonadherent domains, we provide evidence and characterize the purse-string mechanism in the situation where cells do not develop adhesions with their underlying substrate. A model that also involves active epithelial fluctuations describes well the experimental observations.

Author contributions: M.D., P.M., and P.S. designed research; V.N., M.D., G.D., H.G.Y., O.C.-E., and P.M. performed research; V.N., M.D., G.D., H.G.Y., O.C.-E., P.M., and P.S. analyzed data; and V.N., M.D., G.D., H.G.Y., O.C.-E., P.M., and P.S. wrote the paper.

The authors declare no conflict of interest.

This article is a PNAS Direct Submission.

¹V.N., M.D., and G.D. contributed equally to this work.

²To whom correspondence may be addressed. Email: pascal.silberzan@curie.fr or philippe.marcq@curie.fr.

This article contains supporting information online at www.pnas.org/lookup/suppl/doi:10.1073/pnas.1501278112/-DCSupplemental.

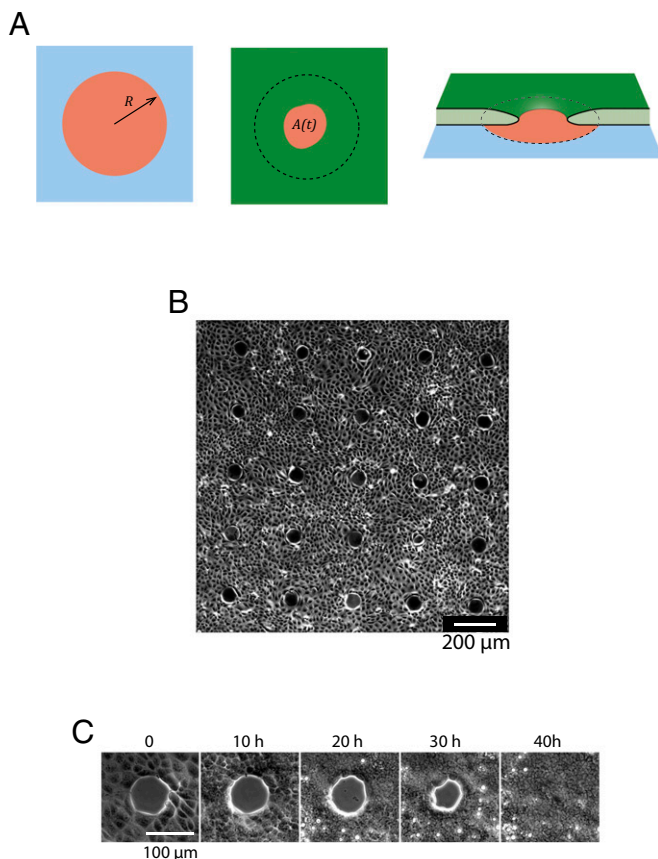


Fig. 1. Fusion of an epithelium over nonadhering domains. (A) Schematics of the experiment: the surface (blue) is patterned with nonadhering domains (red) of radius R . Cells (green) progressively cover these domains and the cell-free area $A(t)$ is dynamically monitored. (B) The 5×5 array of nonadhering domains in phase contrast at the onset of the experiment ($R = 42 \mu\text{m}$). (C) Time evolution of a single domain ($R = 42 \mu\text{m}$).

the same cellular system (22). Tissue fusion was monitored from confluence ($t = 0$) up to 4 d.

Immediately after seeding, the cells adhered on the glass and colonies developed by proliferation. The expanding monolayer readily covered nonadhesive domains that had a radius of less than 10 μm . In these cases, the advancing front edge made no arrest, confirming that cells have the ability to bridge over nonadherent defects smaller than their own size (23–26) (Fig. S1). At the other extreme, for domains with a radius greater than 70 μm , the monolayer covered only the glass surface surrounding the patches (Fig. S1). After several days, we observed the development of a tridimensional “rim” at the boundaries of the domains as already reported (19) but no further evolution in the subsequent weeks (19, 27).

Between these two limiting situations, the monolayer initially surrounded the nonadhesive domains and then proceeded to cover them until it eventually fused (Fig. 1C, Fig. S1, and Movie S1). Observations using confocal microscopy at the nonadherent surface/monolayer interface revealed the absence of vinculin or Paxillin, two proteins associated with focal adhesions. This confirmed our basic assumption: the cells did not develop adhesions with the treated surface during and after closure (Fig. S2).

We followed the closure process by monitoring the area covered by cells on domains of various sizes over a period of several days. A significant fraction of the domains with radii less than $30\text{ }\mu\text{m}$ were already closed when the monolayer reached confluence. Therefore, the mechanism by which cells cover these small domains may be different (for example by direct bridging) from the one relevant to larger domains. As a consequence, we limited our study to $30\text{ }\mu\text{m} < R < 50\text{ }\mu\text{m}$. The cell-free area $A(t)$ showed only minor

distortions to a quasi-circular shape, allowing us to define an effective radius $r(t)$ as $r(t) = \sqrt{A(t)/\pi}$ (Fig. 14).

It is worth comparing the present experiments with the healing of comparable size wounds of the same cell line on homogeneous adhesive substrates in which protrusions at the leading edge were shown to be the driving force for closure (3, 4). In both cases, the shape of the hole remained relatively circular; in particular, no fingering of the leading edge (6) was observed. However, the absence of cell-substrate adhesions drastically slowed down the closing dynamics (typically 30 h in the present setting vs. 3 h on a homogeneously adherent substrate for $R = 35 \mu\text{m}$). Moreover, in the experiments described here, the closing was very “noisy” in two respects. First, a given hole closed in a seemingly erratic succession of large amplitude retractions and expansions of the open area (Fig. 24). In some experiments, we observed closure down to 20% of the initial radius, which then reopened to 50% before eventually closing. However, once the closure was fully completed, there was no reopening (and no indication of a different morphology of the cells over the nonadhesive patch compared with the adhesive surface; Fig. 1C). Second, comparing several closure events for the same nonadhesive patch size, we observed a very large dispersion of the closure times (Fig. 2 C–G and Fig. S3). For instance, if $R = 35 \mu\text{m}$, the average closing time was 44 h and the SD was 18 h ($n = 150$). Because of this large dispersion, the entire distributions of the closure times (and therefore meaningful average closure times) after 83 h could be accessed only for patches with a radius less than $35 \mu\text{m}$. Unfortunately, the development of the above-mentioned 3D rim at the border after typically 4 d prevented us from accessing the long-time parts of these distributions for larger domain sizes.

Given this large variability, we chose to reason in terms of the fraction $f(R, t)$ of closed holes at a time t for a given initial radius R . This fraction f is plotted as a function of R after 4 d (Fig. 2H). As previously mentioned, all patches with a radius less than 35 μm closed within 83 h. By contrast, only a small fraction of the experiments performed at $R > 55 \mu\text{m}$ closed in this time frame. As a matter of fact, we never observed the closing of patches with a radius larger than 70 μm . The full dynamic evolution of these fractions is plotted as a heat map in Fig. 3A for $30 \mu\text{m} < R < 50 \mu\text{m}$ and $0 < t < 83 \text{ h}$.

Closure is necessarily a collective effect as cells must form a continuous structure that bridges over the nonadherent surface. Indeed, by conducting the experiments in low calcium conditions that disrupt cadherin-mediated cell-cell adhesions (19), the efficiency of closure was considerably reduced (Fig. S4).

No stable lamellipodial protrusions similar to those observed on adherent surfaces were evidenced in the present experiments. Moreover, confocal imaging confirmed the presence of a pluricellular actomyosin cable at the edge of the closing open area (Fig. 4A). The contractility of this cable was tested with two-photon laser photo-ablation experiments and by inhibiting myosin II with blebbistatin. When severed, the cable retracted within a few tens of seconds (Fig. 4B and C and [Movie S2](#)), indicating that it is under mechanical tension. By contrast, when the epithelium bridging over the nonadherent surface was punctured after closure, the hole did not expand upon ablation, indicating that no significant tension is stored in the monolayer itself. These small wounds then closed rapidly by developing protrusions presumably on the debris left by the ablation. Furthermore, the addition of blebbistatin almost completely inhibited closure ([Fig. S4](#)), whereas the same conditions have been shown to slow down but not halt closure on homogeneous adherent surfaces (4).

Our observations confirm that, as the cells do not interact with the surface in our experiments, the contractile pluricellular actomyosin cable along the edge must contract and pull the tissue over the adhesion-free surface by a purse-string mechanism. By contrast, the tension in the epithelium itself is not a factor in this process.

To describe these experiments, we wrote the force balance equation at the free edge, on a line element of the contractile cable of radius $r(t)$. As ingredients of the equation, we considered (Fig. S5): (i) a force $f_{\text{cable}} = -\frac{\gamma}{r}$ due to the line tension γ of the contractile cable, similar to what has been proposed to

describe the shape of single cells anchored to the surface via discrete points (28, 29); (ii) a friction force $f_{\text{friction}} = -\xi \frac{dr}{dt}$ where ξ is a friction coefficient encapsulating the dissipative processes at the cable and between cells (there is no interaction and hence no friction at the monolayer/substrate interface); and (iii) a stochastic force f_{noise} needed to model the above-described stochastic effects, such as the wide distributions of closing times (Fig. 2 C–G and Fig. S3) or the very noisy trajectories (Fig. 2A). As puncturing the epithelium did not result in opening of the wound, we initially did not include epithelial tension in our description (see below). After dividing the force balance equation by the friction coefficient ξ , the Langevin equation describing the evolution of the radius $r(t)$ reads (Supporting Information, Part A) (30):

$$\frac{dr}{dt} = -\frac{\tilde{\gamma}}{r} + \sqrt{2D} \cdot \eta(t), \quad [1]$$

where $\tilde{\gamma} = \gamma/\xi$ and $\sqrt{2D}\eta(t)$ is a noise term where the diffusion coefficient D quantifies the amplitude of radius fluctuations at the margin. Note that ignoring orthoradial force balance is supported by independent force measurements on keratinocytes, showing that, close to the free edge, the radial component of the traction stress remained large compared with the orthoradial component during closure (17).

For the sake of simplicity, we further assumed that (i) $\eta(t)$ is a Gaussian white noise with an autocorrelation function $\langle \eta(t)\eta(t') \rangle = \delta(t-t')$, and that (ii) γ , ξ , and D remained constant (independent of r and t). Note that a constant diffusion coefficient D corresponds to fluctuations $\Delta\sigma$ of the epithelial tension σ about its average value (zero in the present case): $D = \frac{\Delta\sigma^2}{2\xi^2}$ (see below).

During the early stages of fusion, Eq. 1 reduces to simple diffusion, and the initial mean square deviation reads (Supporting Information, Part D):

$$\langle (r(0) - r(t))^2 \rangle_{t \rightarrow 0} = 2Dt. \quad [2]$$

The experimental data were in good agreement with this theoretical expression, yielding $D = 1.56 \pm 0.03 \mu\text{m}^2 \text{h}^{-1}$ (Fig. 2I) and confirming a diffusive behavior of the radius at short times. Hence, the cable tension γ does not contribute to the initial statistics that are fully determined by the fluctuations.

In this framework, the fraction of closed wounds $f(R, t)$ obeyed a backward Fokker–Planck (Supporting Information, Part A):

$$\frac{\partial}{\partial t} f(R, t) = -\frac{\tilde{\gamma}}{R} \frac{\partial}{\partial R} f(R, t) + D \frac{\partial^2}{\partial R^2} f(R, t), \quad [3]$$

which could be solved numerically for a given set of parameters and with boundary conditions in accord with our experimental observations: We imposed that $r = R$ was a reflecting boundary (a hole never opened beyond the area of the nonadhesive domain) and $r = 0$ was absorbing (there was no reopening after full closure). The closure time was then the time at which $r = 0$ was first attained (first-exit time).

A least squares method allowed us to fit the model to the data over the whole map of the fraction of closed wounds (31). Varying R and t at given $\tilde{\gamma}$ and D , we minimized the mean square standardized error between the theoretical frequencies and experimental fractions (see Supporting Information, Part C for the definition of the error function and a full description of the fitting procedure). This fit yielded the following estimates of the parameters (Fig. 3B):

$$\tilde{\gamma} = 10 \mu\text{m}^2 \text{h}^{-1} [6, 13]; D = 1.6 \mu\text{m}^2 \text{h}^{-1} [0.5, 3.9],$$

where the numbers between brackets give the 95% confidence interval (Fig. 3C). Note that the diffusion coefficient is consistent with our previous estimate based on the short-time evolution of

the closure (Fig. 2I). With these parameters, the simulated and experimental fractions seemed very similar as can be seen in Fig. 3A and B. More quantitatively, the particular case of the closure half-time at which 50% of the domains have closed as well as the distributions of closure times for various radii were indeed well described by this set of parameters (Figs. 3D and 2 C–G and Supporting Information, Part C). Finally, trajectories simulated from Eq. 1 (32) with the previously determined values of $\tilde{\gamma}$ and D closely resembled the experimental ones (Fig. 2A and B).

Altogether, we conclude that our stochastic model provides a self-consistent description of the closure dynamics. As the confidence intervals for D and $\tilde{\gamma}$ exclude 0, the description is also minimal in the sense that none of the components can be removed from the description.

Discussion

We have provided evidence that a cell monolayer can develop over nonadherent surfaces even when cells at the edge are not anchored to a substrate to pull on it. This property is the transposition at the tissue scale of a single cell's ability to bridge over defects smaller than its own size. Experiments conducted in low calcium conditions or in presence of Blebbistatin show that such closures are the result of a collective behavior and that impairing the actomyosin contractility, in particular at the purse-string cable, affects this process.

The experimental results are well described by a stochastic model that includes the tension γ of the circumferential actomyosin cable, an effective friction ξ and the amplitude D of the fluctuations of the radius reflecting the ones of the epithelial tension. Our theory therefore emphasizes the role and function of the purse-string contractility under these conditions. Interestingly, this purse-string mechanism is secondary to lamellipodial protrusions when the same MDCK cells are migrating on surfaces on which they can develop adhesions (3). As MDCK cells develop a peripheral actomyosin cable in both these situations, we conclude that the nature of the substrate on which cells migrate controls whether this cable has a regularization or a purse-string function.

From a typical value of the cable tension $\gamma \sim 1 - 10 \text{ nN}$ (25, 33), the order of magnitude of the (one-dimensional) friction coefficient is $\xi \sim 0.1 - 1 \text{ nN } \mu\text{m}^{-2} \text{h}$. We can compare this value with the hydrodynamic 2D friction coefficient measured for the same cells in a similar setting but on an adherent substrate (3): $\xi_{\text{adh}} \sim 10^{-3} \text{ nN } \mu\text{m}^{-3} \text{h}$. The characteristic length defined as $\frac{\xi}{\xi_{\text{adh}}}$, is typically 100–1,000 μm , consistent with the correlation length characterizing the collective migration of MDCK cells on glass (3, 22). Therefore, it is likely that the friction term originates mostly from the monolayer adhering to the glass around the nonadhesive domains.

An important (and intuitively unexpected) conclusion of our study is that fluctuations actively contribute to closing. This is particularly apparent at the onset of closing (short times) where fluctuations are actually the dominant term in the closure dynamics (Eq. 2). Theoretical average closure times can be analytically computed as first-exit times and we obtain for the average closure time $\langle t_c(R) \rangle = R^2/2(\tilde{\gamma} + D)$ (Supporting Information, Part C), which shows immediately that, in a statistical sense, a nonzero diffusion coefficient accelerates the closure. The model further predicts that the SD of the closure time is proportional to and of same order as the average value (Supporting Information, Parts C and D). Quantitatively, within our limited dynamical range, these predictions are borne out by data with the fitted parameters determined previously (Fig. 2 F and G). Last, we validate one of our hypotheses of a white noise in the diffusive term of the Langevin Eq. 1. We used the model, and the fitted parameters, to measure the experimental noise, and checked that the autocorrelation function of this noise decays rapidly with time, with a correlation time of the order of an hour (Fig. S6). Because experiments are performed over days, this confirms that the white noise approximation is indeed appropriate.

We then checked whether our initial assumption of not including the epithelial tension in Eq. 1, initially based on tissue photoablation experiments, could be further confirmed. A nonzero

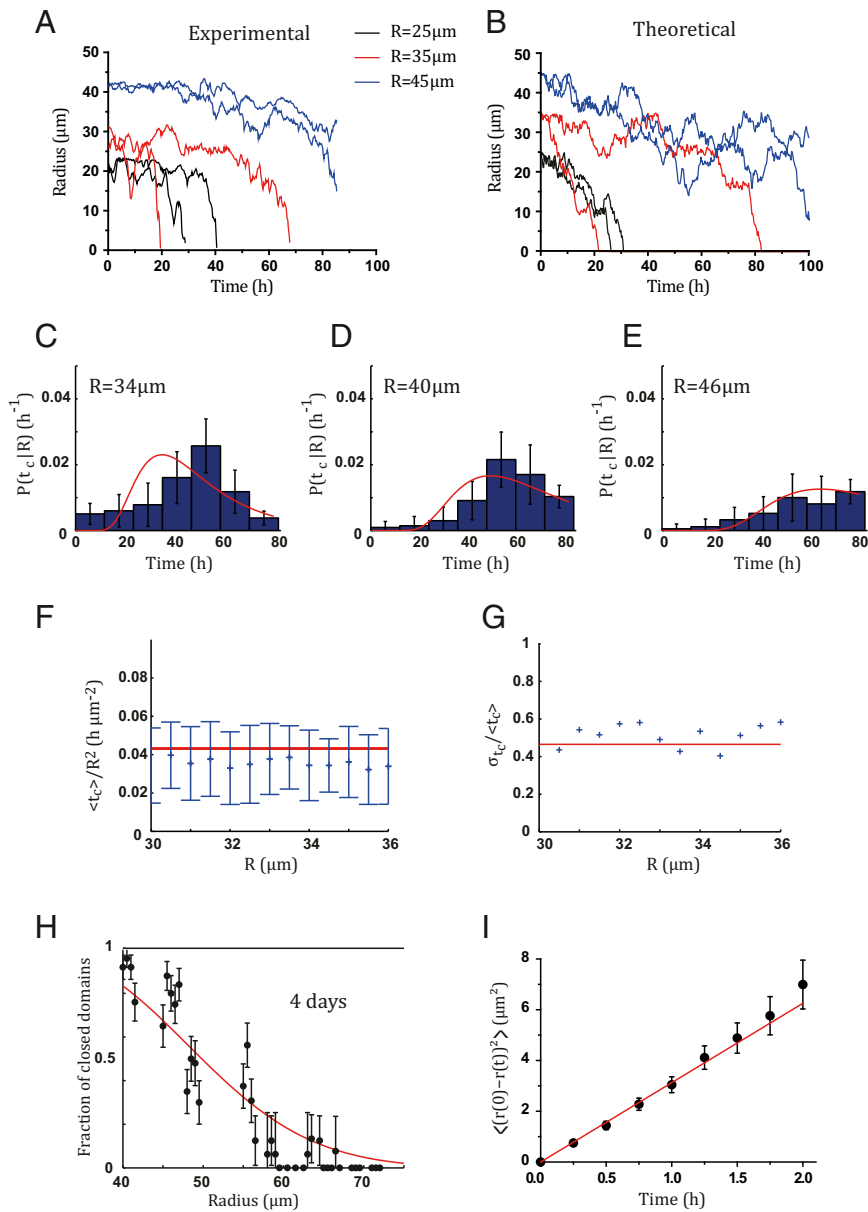


Fig. 2. Gap closure is a stochastic process. Comparison between experimental (A) and theoretical (B) trajectories. The two are visually very close. Note the very large fluctuations of the radius during closure. (C–E) The closure times are widely distributed for a given initial radius (bars: experimental values, lines theoretical predictions with $\tilde{\gamma} = 10 \mu\text{m}^2 \text{h}^{-1}$ and $D = 1.6 \mu\text{m}^2 \text{h}^{-1}$). Error bars are SEMs. N values are 571 (C), 498 (D), and 498 (E). (F) As predicted by the model, the ratio $\langle t_c \rangle / R^2$ is approximately constant within the accessible dynamical range $30 \leq R \leq 36 \mu\text{m}$, where long time closure events ($t_c > 84 \text{ h}$) are negligible. The red line corresponds to the theoretical prediction (Eq. S37) $\langle t_c \rangle / R^2 = \frac{1}{2(\tilde{\gamma} + D)} = 0.043 \text{ h}/\mu\text{m}^2$ with $\tilde{\gamma} = 10 \mu\text{m}^2/\text{h}$ and $D = 1.6 \mu\text{m}^2/\text{h}$. Error bars are SDs. (G) The coefficient of variation of the closure time is approximately constant within the same range, with values consistent with the theoretical prediction (Eq. S43) indicated with a solid line: $\frac{\sigma_{t_c}}{\langle t_c \rangle} = \sqrt{\frac{2D}{\tilde{\gamma} + D}} = 0.47$ with $\tilde{\gamma} = 10 \mu\text{m}^2/\text{h}$ and $D = 1.6 \mu\text{m}^2/\text{h}$. (H) Fractions of closed wounds at 4 d (black points). The red line is the theoretical fraction ($\tilde{\gamma} = 10 \mu\text{m}^2 \text{h}^{-1}$ and $D = 1.6 \mu\text{m}^2 \text{h}^{-1}$). Error bars are SEMs. (I) Early times are well described by a diffusive process. Points are the experimental points resulting from the average of more than 400 trajectories, the red line is a linear fit yielding a diffusion coefficient of $D = 1.56 \pm 0.03 \mu\text{m}^2 \text{h}^{-1}$ (error bars are SEMs).

tension σ would add a constant term $\tilde{\sigma} = \sigma/\xi$ to the drift coefficient on the right-hand side of the Langevin Eq. 1. As shown in [Supporting Information, Part B](#), analyzing our data with these three parameters ($\tilde{\gamma}, \tilde{\sigma}, D$) yielded a very small (negative) epithelial tension, whereas the two other parameters retained values close to the ones previously determined ([Fig. S7 A and B](#)). Therefore, the epithelial tension can be safely omitted, suggesting that the time scales involved in the fusion process are sufficiently long to allow elastic stresses to relax (34). Not surprisingly, putting $\tilde{\gamma} = 0$ in this new equation led to a drastic decrease of the fraction of closed wounds at 83 h in good agreement with our experimental observations in presence of blebbistatin ([Fig. S4](#)).

Next, we asked whether including fluctuations of the cable tension would better describe our experimental data than our current hypothesis in which these fluctuations arise only from the epithelial tension (D independent of r). Assuming for simplicity that fluctuations in the monolayer tension and in the cable tension are not correlated, we expressed the diffusion coefficient as $D_{\text{tot}}(r) = D + D_\gamma/r^2$ where D and D_γ are proportional to the (constant) amplitudes of the fluctuations of these two tensions. Fitting model to data within a 3D parameter space ($\tilde{\gamma}, D, D_\gamma$)

allowed us to conclude that fluctuations in the cable tension could be ignored except for values of r much smaller than a cell size ([Supporting Information, Part C](#) and [Fig. S7 C and D](#)). Of note, at these very small radius values ($r < 1 \mu\text{m}$), the fluctuations of the cable become dominant over both the fluctuations of the epithelial tension and the deterministic cable tension ([Supporting Information, Part B](#)). This regime corresponds to the very late stages of closure, which are, unfortunately, beyond our experimental time resolution. Apart from this regime, the noise term of the stochastic model therefore originates from fluctuations of the monolayer tension about its zero mean value. These fluctuations result from cell-level dynamics occurring over short time scales, such as rearrangements, divisions, or cells being pulled out from the adhesive part.

From the typical value of ξ determined above, we can also estimate the magnitude of the active fluctuations of the epithelial tension: $\Delta\sigma_{\text{active}}^2 = 2D\xi^2 \sim 10^{-2} - 1 \text{ nN}^2 \mu\text{m}^{-2} \text{h}$. This is, to our knowledge, the first experimental measurement of this quantity. We can compare this value to the amplitude of tension fluctuations resulting from thermal noise: $\Delta\sigma_{\text{thermal}}^2 = 2D_{\text{thermal}}\xi^2$. As the total friction of the cable over its perimeter is $2\pi R\xi$, the

polyethyleneglycol (PEG) to which cells do not adhere (18, 19, 38). Domains whose radii were between 5 and 75 μm with a 0.5- μm increment were defined by photolithography directly on the coating in such a way that it remained protected by the photoresist (S1813; Microchem) at the desired location of the nonadhesive domains (19). Using the photoresist as an etching mask, the PEG coating was removed in the photoresist-free areas with an air plasma (Harrick plasma cleaner), revealing the underlying glass. The resist was then dissolved leading to PEG-coated domains surrounded by a clean glass surface. The surface treatment was stable for weeks in biological buffers (19).

Cell Culture. MDCK cells (39) were cultured in DMEM supplemented with 10% FBS (Sigma), 2 mM L-glutamin solution (Gibco), and 1% antibiotic solution [penicillin (10,000 units/mL), streptomycin (10 mg/mL)]. Cells were seeded and maintained at 37 °C, 5% CO₂, and 90% humidity throughout the experiments. We also used MDCK LifeAct cells (3) for ablation experiments [these clones were cultured in presence of geneticin (400 $\mu\text{g/mL}$)].

Blebbistatin (Sigma) was used at a concentration of 50 μM . Experiments were started in the absence of the drug. At confluence, a fraction of the supernatant was pumped out, mixed with the drug, and reinjected into the well.

Low-calcium medium (calcium-free DMEM, FBS 10%, Penstrep 1%, 50 mM calcium) was used to reduce cell–cell adhesion. Experiments were started in regular DMEM and the buffer was changed to low-calcium DMEM at confluence.

Microscopy and Data Analysis. The bottoms of Petri dishes or 6-well plates were replaced with patterned glass slides. Cells were imaged in phase contrast on an Olympus IX71 inverted microscope equipped with temperature, CO₂ and humidity regulation (LIS), a motorized stage for multipositioning (Prior), and a Retiga 4000R camera (QImaging). Unless otherwise specified, a 10X objective was used and images were acquired every 30 min. Displacements and image acquisition were computer-controlled with Metamorph (Molecular Devices).

Fixed fluorescently marked cells were observed under an upright Imager Z2 spinning disk microscope (Zeiss) equipped with a CoolSnapHQ2 camera

(Photometrics) and a 63X water immersion objective. All acquisitions were controlled using MetaMorph software (Molecular Devices).

Images were processed with the ImageJ software (40) or with Matlab (MathWorks) routines. Further analysis was occasionally performed on Origin (OriginLab).

Unless otherwise specified, fractions of closed wounds were computed from at least 100 domains for each size measured over at least four distinct experiments.

Laser Ablations. Photoablation experiments were performed on an LSM 710 NLO (Zeiss) microscope equipped with a two-photon MaiTai laser and a 40X oil immersion objective. The two-photon laser was used at 85% power and at a wavelength of 890 nm.

Immunofluorescence. Cells were fixed in 4% PFA, permeabilized in 0.1% Triton X-100 and blocked in 10% FBS in PBS. Vinculin labeling was performed with a mouse monoclonal anti-vinculin antibody (Sigma; 1:500) and Paxillin labeling was performed with a mouse anti-paxillin antibody (Sigma; 1:500) both followed by Alexa 488 donkey anti-mouse (Life Technologies; 1:500). Actin was labeled using Alexa 546 phalloidin (Life Technologies; 1:1,000). Myosin was labeled with rabbit anti-phospho myosin light chain (Ozyme; 1:100) followed by Alexa 488 chicken anti-rabbit (Life Technologies; 1:1,000). Hoescht 33342 (Sigma; 1:10,000) was used to mark the nuclei.

ACKNOWLEDGMENTS. We gratefully thank Isabelle Bonnet, Axel Buguin, Nir Gov, Jonas Ranft, and all the members of the “biology-inspired physics at mesoscales” group for discussions, as well as Gabriel Dumy for performing part of the analysis. The “biology inspired physics at mesoscales” group and the “physical approaches of biological problems” group are part of the CellTisPhysBio Labex. We acknowledge financial support from the Programme Incitatif et Coopératif Curie “Modèles Cellulaires”. H.G.Y. thanks the Fondation Pierre-Gilles de Gennes for financial support. We acknowledge the Cell and Tissue Imaging Platform (member of France-Bioimaging) of the Genetics and Developmental Biology Department (UMR3215/U934) of Institut Curie and in particular Olivier Renaud and Olivier Leroy.

- Ray HJ, Niswander L (2012) Mechanisms of tissue fusion during development. *Development* 139(10):1701–1711.
- Martin P (1997) Wound healing—Aiming for perfect skin regeneration. *Science* 276(5309):75–81.
- Cochet-Escartin O, Ranft J, Silberzan P, Marcq P (2014) Border forces and friction control epithelial closure dynamics. *Biophys J* 106(1):65–73.
- Anon E, et al. (2012) Cell crawling mediates collective cell migration to close undamaged epithelial gaps. *Proc Natl Acad Sci USA* 109(27):10891–10896.
- Brugués A, et al. (2014) Forces driving epithelial wound healing. *Nat Phys* 10:683–690.
- Reffay M, et al. (2014) Interplay of RhoA and mechanical forces in collective cell migration driven by leader cells. *Nat Cell Biol* 16(3):217–223.
- Abreu-Blanco MT, Verboon JM, Liu R, Watts JJ, Parkhurst SM (2012) Drosophila embryos close epithelial wounds using a combination of cellular protrusions and an actomyosin purse string. *J Cell Sci* 125(Pt 24):5984–5997.
- Copp AJ, Brook FA, Estibeiro JP, Shum AS, Cockcroft DL (1990) The embryonic development of mammalian neural tube defects. *Prog Neurobiol* 35(5):363–403.
- Bement WM, Mandato CA, Kirsch MN (1999) Wound-induced assembly and closure of an actomyosin purse string in *Xenopus* oocytes. *Curr Biol* 9(11):579–587.
- Kiehart DP (1999) Wound healing: The power of the purse string. *Curr Biol* 9(16):R602–R605.
- Jacinto A, Martinez-Arias A, Martin P (2001) Mechanisms of epithelial fusion and repair. *Nat Cell Biol* 3(5):E117–E123.
- Hutson MS, et al. (2003) Forces for morphogenesis investigated with laser microsurgery and quantitative modeling. *Science* 300(5616):145–149.
- Friedl P, Locker J, Sahai E, Segall JE (2012) Classifying collective cancer cell invasion. *Nat Cell Biol* 14(8):777–783.
- Curtis AS, Varde M (1964) Control of cell behavior: Topological factors. *J Natl Cancer Inst* 33:15–26.
- Vedula SRK, et al. (2014) Epithelial bridges maintain tissue integrity during collective cell migration. *Nat Mater* 13(1):87–96.
- Gautrot JE, et al. (2012) Mimicking normal tissue architecture and perturbation in cancer with engineered micro-epidermis. *Biomaterials* 33(21):5221–5229.
- Vedula SRK, et al. (2015) Mechanics of epithelial closure over non-adherent environments. *Nat Commun* 6:6111.
- Tourovskaya A, Figueroa-Masot X, Folch A (2006) Long-term microfluidic cultures of myotube microarrays for high-throughput focal stimulation. *Nat Protoc* 1(3):1092–1104.
- Deforet M, Hakim V, Yevick HG, Duclos G, Silberzan P (2014) Emergence of collective modes and tri-dimensional structures from epithelial confinement. *Nat Commun* 5:3747.
- Underhill GH, Galie P, Chen CS, Bhatia SN (2012) Bioengineering methods for analysis of cells in vitro. *Annu Rev Cell Dev Biol* 28:385–410.
- Harris AR, et al. (2012) Characterizing the mechanics of cultured cell monolayers. *Proc Natl Acad Sci USA* 109(41):16449–16454.
- Petitjean L, et al. (2010) Velocity fields in a collectively migrating epithelium. *Biophys J* 98(9):1790–1800.
- Geiger B, Spatz JP, Bershadsky AD (2009) Environmental sensing through focal adhesions. *Nat Rev Mol Cell Biol* 10(1):21–33.
- Bischofs IB, Safran SA, Schwarz US (2004) Elastic interactions of active cells with soft materials. *Phys Rev E Stat Nonlin Soft Matter Phys* 69(2 Pt 1):021911.
- Guthardt Torres P, Bischofs IB, Schwarz US (2012) Contractile network models for adherent cells. *Phys Rev E Stat Nonlin Soft Matter Phys* 85(1 Pt 1):011913.
- Rossier OM, et al. (2010) Force generated by actomyosin contraction builds bridges between adhesive contacts. *EMBO J* 29(6):1055–1068.
- Kim JH, et al. (2013) Propulsion and navigation within the advancing monolayer sheet. *Nat Mater* 12(9):856–863.
- Bar-Ziv R, Tlsty T, Moses E, Safran SA, Bershadsky A (1999) Pearling in cells: A clue to understanding cell shape. *Proc Natl Acad Sci USA* 96(18):10140–10145.
- Bischofs IB, Klein F, Lehnert D, Bastmeyer M, Schwarz US (2008) Filamentous network mechanics and active contractility determine cell and tissue shape. *Biophys J* 95(7):3488–3496.
- Gardiner WC (2004) *Handbook of Stochastic Methods for Physics, Chemistry and the Natural Sciences* (Springer, Berlin).
- Bevington PR, Robinson DK (1969) *Data Reduction and Error Analysis for the Physical Sciences* (McGraw-Hill, New York).
- Kloedel P, Platen E (1999) *Numerical Simulations of Stochastic Differential Equations* (Springer, Berlin).
- Yoshinaga N, Marcq P (2012) Contraction of cross-linked actomyosin bundles. *Phys Biol* 9(4):046004.
- Ranft J, et al. (2010) Fluidization of tissues by cell division and apoptosis. *Proc Natl Acad Sci USA* 107(49):20863–20868.
- Douezan S, Brochard-Wyart F (2012) Active diffusion-limited aggregation of cells. *Soft Matter* 8:784–788.
- Martin E, Behn U, Germano G (2011) First-passage and first-exit times of a Bessel-like stochastic process. *Phys Rev E Stat Nonlin Soft Matter Phys* 83(5 Pt 1):051115.
- Yevick HG, Duclos G, Bonnet I, Silberzan P (2015) Architecture and migration of an epithelium on a cylindrical wire. *Proc Natl Acad Sci USA* 112(19):5944–5949.
- Tourovskaya A, et al. (2003) Micropatterns of chemisorbed cell adhesion-repellent films using oxygen plasma etching and elastomeric masks. *Langmuir* 19:4754–4764.
- Belluscì S, Moens G, Thiery J-P, Jouanneau J (1994) A scatter factor-like factor is produced by a metastatic variant of a rat bladder carcinoma cell line. *J Cell Sci* 107(Pt 5):1277–1287.
- Rasband WS (1997) ImageJ (National Institutes of Health, Bethesda, MD). Available at imagej.nih.gov/ij. Accessed July 9, 2015.